Towards Gradient-Based Actuation of Magnetic Soft Robots Using a Six-Coil Electromagnetic System

Venkatasubramanian Kalpathy Venkiteswaran, *Member, IEEE* and Sarthak Misra, *Member, IEEE*

***Abstract*— Soft materials with embedded magnetic properties can be actuated in a contactless manner for dexterous motion in restricted and unstructured environments. Magnetic soft robots have been demonstrated to be capable of versatile and programmable untethered motion. However, magnetic soft robots reported in literature are typically actuated by utilizing magnetic fields to generate torques that produce deformation. By contrast, this work investigates the utilization of field gradients to produce tethering forces for anchoring soft robots to the working surface, in conjunction with the use of magnetic fields to generate torques for deformation. The methodology applied here uses a six-coil electromagnetic system for field generation. The approach to achieve the magnetic field and gradients desired for soft robot motion is described, along with the restrictions imposed by Maxwell's equations. The design and fabrication of the soft robots is explained together with calculations to assess the capabilities of the actuation system. Proof-of-concept demonstrations of soft robot motion show *Hexapede* robots with the ability to 'walk' untethered on the ceiling of the workspace, working against gravity; and lightweight *Worm* robots made of thin strips of material are demonstrated to locomote while staying in contact with the ground.**

I. INTRODUCTION

In recent years, the use of soft materials within robotic devices has gained widespread traction due to their beneficial structural properties such as flexibility and resilience [1]. In contrast to rigid-body robots, soft robots conform to their environment, making them suitable for specific tasks such as maneuvering in tight and unstructured spaces, and grasping delicate objects [2]. Soft robotic systems are generally under-actuated (due to the flexibility in the material) with low-level primitives (e.g., motion gaits, grasping poses) built into the structure, while control is achieved using a few high-level actuation inputs (e.g., pneumatic, electric) [3], [4]. However, in order to use soft robots reliably for real-world applications, there is a need to develop actuation and control techniques that accentuate the structural benefits while stabilizing the low-level primitives; for instance, anchoring locomoting robots to a working surface in order to overcome gravity or other environmental conditions.

Magnetic soft robots are actuated using magnetic fields, which enables contactless transfer of power from actuator to the robot [5]. These soft robots are fabricated using magnetic polymer composites (MPC) which consist of ferromagnetic particles embedded into a polymeric material (rubbers, resins etc.) [6]. A large magnetization field is used to align the magnetic dipoles within the MPC during the fabrication process [7]. This gives the material a 'memory' of the magnetization shape, which can be exploited to produce deformation in the material by controlling the actuating field [8]. Magnetic soft robots are of particular interest in the field of minimally invasive surgery because magnetic fields are not harmful to humans, and the robots can operate in small, restricted spaces in an untethered manner [9], [10]. In previous work, we demonstrated biomimetic terrestrial locomotion of multi-limbed magnetic soft robots [11].

The actuating field for magnetic soft robots can be generated using permanent magnets or electromagnetic coils, and the rated power of the magnets defines the limits of the workspace. Magnetic actuation systems have been developed with stationary electromagnetic coils [12], [13], coils on moving frames [14], coils or permanent magnets on serial robots [15], [16], and permanent magnets on closed-chain mechanisms [17]. Permanent magnets can provide high fields, but the generated field is constant and the actuation is achieved by controlling the pose of the magnet with respect to the robot workspace. Electromagnetic coils allow the control of field magnitude through the input current, offering more degrees of freedom in actuation, but can suffer from heating problems and scalability issues [15].

When an MPC is subjected to an external actuation field, the dipoles in the structure try to align with the external field, generating an internal torque that causes bending deformation of the structure. Simultaneously, magnetic fields also produce forces that attract (or repel) the dipoles in the MPC towards (or away from) the source of the field. With permanent magnets, Simi *et al.* have demonstrated dragging of an endoscopic device along the abdominal wall [18], while Pittiglio *et al.* used magnetic levitation to control the position of a capsule within the colon [19]. Electromagnetic coils have also been used to achieve combined force and torque control on neutrally-buoyant microrobots [20], [21]. By contrast, most of the work on magnetic soft robots only takes into account the bending deformation caused by the internal torque to produce motion of the soft robots.

This work aims to exploit the attractive forces generated by a magnetic field to anchor soft robots to a working surface. Using this approach, it is possible to create soft robots that can operate on inclined, vertical or inverted surfaces (walls, ceilings etc.), working against gravity, buoyancy or other environmental conditions. The novelty of this work

The authors are affiliated with Surgical Robotics Laboratory, Department of Biomechanical Engineering, University of Twente, Enschede, The Netherlands. S. Misra is also affiliated with Department of Biomedical Engineering, University of Groningen and University Medical Centre Groningen, Groningen, The Netherlands.

This research has received funding from the European Research Council (ERC) under the European Union's Horizon 2020 Research and Innovation programme (Grant Agreement #638428 - project ROBOTAR).

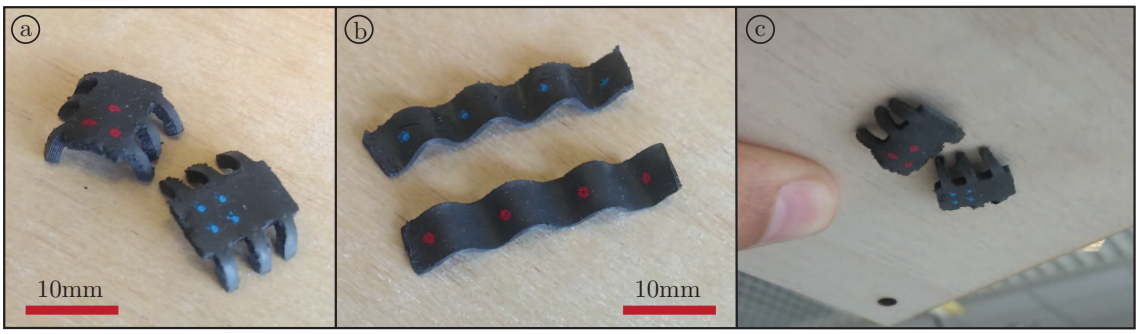

Fig. 1: Examples of soft robots fabricated using a magnetic polymer composite (MPC), and designed for actuation using combination of magnetic force and torque. ⓐ *Hexapede* robots. ⓑ *Worm* robots. ⓒ *Hexapede* robots anchored to a wooden surface against gravity using magnetic force generated by a permanent magnet (not shown).

lies in the combined use of magnetic forces and torques generated by electromagnetic coils to control soft robotic devices. Bioinspired designs of soft robots that locomote with and without limbs are detailed (Fig. 1). The magnetic field generation principle is described, specifically in the context of the six-coil electromagnetic system used here. The robots are fully magnetic, requiring no other stimulus for motion. The motion of the robots while being anchored to the working surface is demonstrated as a proof-of-concept. Finally, the limitations of the current approach are discussed, along with possible directions for future work.

II. MAGNETIC FIELD GENERATION

In this section, the fundamentals of magnetic fields are described first, followed by the method of generating forces and torques to actuate the soft robots. While the theory described here is specific to the actuation unit being used, the basic methodology can be applied to generic electromagnetic coil systems.

A. Magnetic actuation

Consider a magnetic field ($\mathbf{B} \in \mathbb{R}^3$) in a workspace with zero current density in the working medium (typically the case in a manipulation space) [22]. Maxwell's equations say that the divergence and curl of the magnetic field in such a case are zero, or,

$$\nabla \cdot \mathbf{B} = 0, \tag{1}$$

$$\nabla \times \mathbf{B} = 0. \tag{2}$$

This imposes constraints on the field gradient matrix, necessitating it to be symmetric and have zero trace. Therefore, in a standard Cartesian coordinate system

$$\nabla \mathbf{B} = \begin{bmatrix} \frac{\partial B_x}{\partial x} & \frac{\partial B_x}{\partial y} & \frac{\partial B_x}{\partial z} \\ \frac{\partial B_x}{\partial y} & -\left(\frac{\partial B_x}{\partial x} + \frac{\partial B_z}{\partial z}\right) & \frac{\partial B_z}{\partial y} \\ \frac{\partial B_x}{\partial z} & \frac{\partial B_z}{\partial y} & \frac{\partial B_z}{\partial z} \end{bmatrix}. \tag{3}$$

where B_x, B_y and B_z denote the components of $\mathbf{B}$ in the x, y, z directions, respectively. An object with magnetic dipole moment ($\mu \in \mathbb{R}^3$) within this field experiences a force ($\mathbf{F}_\mu \in \mathbb{R}^3$) and a torque ($\mathbf{T}_\mu \in \mathbb{R}^3$) given by

$$\mathbf{F}_\mu = \mu \cdot \nabla \mathbf{B}, \tag{4}$$

$$\mathbf{T}_\mu = \mu \times \mathbf{B}. \tag{5}$$

This torque and force can be used to manipulate the soft robots to achieve motion.

B. Electromagnetic coil system

The magnetic field and gradients used to control the soft robots in this work are generated using a system of six electromagnetic coils called BigMag [14]. It has six electromagnetic coils on two rotating frames (Fig. 2). The working area in the center is a sphere of about 10cm in diameter. The system has an operating frequency of up to 40Hz and has cameras for recording experiments at 30FPS. For the experiments here, a circular workspace is made with an Acrylonitrile Butadiene Styrene (ABS) base and an acrylic ceiling for the tests. The current to each coil can be controlled independently, as can the rotation of the two frames.

At a given point ($\mathbf{p} \in \mathbb{R}^3$) within the workspace, the contribution of each coil (k = 1,2,...6) towards the total magnetic field can be calculated using a unit field map ($\beta_k(\mathbf{p}, \boldsymbol{\theta}) \in \mathbb{R}^3$) as

$$\mathbf{B}_k(\mathbf{p}) = I_k \beta_k(\mathbf{p}, \boldsymbol{\theta}), \tag{6}$$

where $I_k \in \mathbb{R}$ is the current in the k^{th} coil, and $\boldsymbol{\theta} \in \mathbb{S}^2$ represents the positions of the rotating coil frames. Similarly, the contribution of each coil to the field gradient is given by the unit field gradient map ($\gamma_k(\mathbf{p}, \boldsymbol{\theta}) \in \mathbb{R}^9$), such that

$$\nabla \mathbf{B}_k(\mathbf{p}) = I_k \gamma_k(\mathbf{p}, \boldsymbol{\theta}). \tag{7}$$

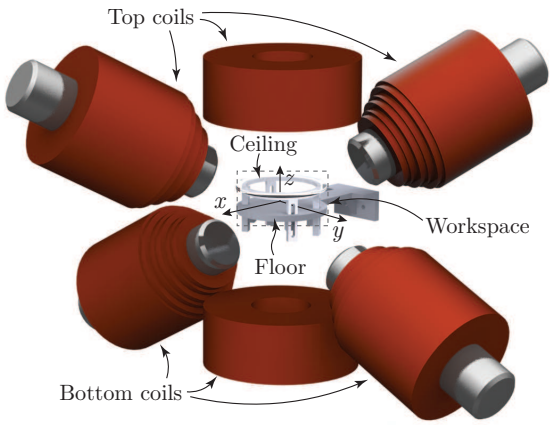

Fig. 2: Schematic of actuation setup and experimental workspace used for experiments. The actuation unit (BigMag [14]) consists of six electromagnetic coils. The experiment workspace is made from 3D-printed Acrylonitrile Butadiene Styrene (ABS), with a transparent acrylic ceiling.

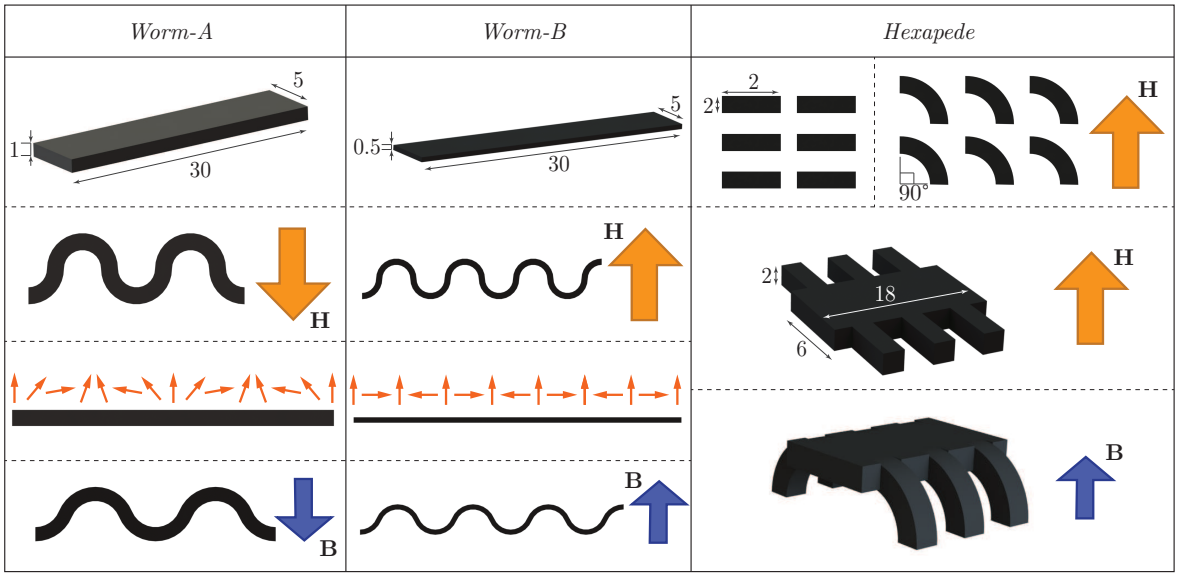

Fig. 3: The fabrication process of the soft robots requires curing a magnetic polymer composite (MPC) in the shape of the robot, followed by magnetization. *Worm-A* and *Worm-B* are made of flat strips of MPC. They are magnetized under a large field (**H**), which aligns the magnetic dipoles (orange arrows) as shown. Upon application of a smaller actuation magnetic field (**B**), the material deforms to align the dipoles to the external field. For *Hexapede*, the legs are fabricated and magnetized in the form of quarter circles, after which they are combined with the body. Then, the whole robot is magnetized, but the dipoles in the legs maintain their initial alignment. Under actuation, the legs bend into the quarter circle shape, lifting the robot. All dimensions are in mm.

Therefore, the total field and gradient at $\mathbf{p}$ are given by

$$\mathbf{B}(\mathbf{p}) = [\beta_1(\mathbf{p},\boldsymbol{\theta}), \beta_2(\mathbf{p},\boldsymbol{\theta}), \ldots, \beta_6(\mathbf{p},\boldsymbol{\theta})]\,\mathbf{I} \quad (8)$$

$$\nabla\mathbf{B}(\mathbf{p}) = [\gamma_1(\mathbf{p},\boldsymbol{\theta}), \gamma_2(\mathbf{p},\boldsymbol{\theta}), \ldots, \gamma_6(\mathbf{p},\boldsymbol{\theta})]\,\mathbf{I}, \quad (9)$$

where $\mathbf{I} = [I_1, I_2, \ldots I_6]$. Details on derivation of the unit field maps can be found in Sikorski *et al.* [14].

C. Combined field and gradient generation

The framework used in this paper for combined field and gradient generation is described in this section. The discussion here is limited to only consider torques causing bending in the x-z plane and forces in the z-direction, for demonstrating proof-of-concept. Therefore, in (8) and (9), only those components of the unit field map that relate to the aforementioned loads are included. From (4) and (5),

$$\begin{bmatrix} F_\mu^z \\ T_\mu^y \end{bmatrix} = \begin{bmatrix} \frac{\partial B_z}{\partial x} & \frac{\partial B_z}{\partial y} & \frac{\partial B_z}{\partial z} \\ -B_z & 0 & B_x \end{bmatrix} \begin{bmatrix} \mu_x \\ \mu_y \\ \mu_z \end{bmatrix} = \widetilde{\mathbf{B}}\,\mu. \quad (10)$$

Additionally, the coils of BigMag are kept stationary, meaning $\boldsymbol{\theta} = [0, 0]$. Therefore, in order to control the five non-zero elements of $\widetilde{\mathbf{B}}$, the only actuation inputs are the currents to the coils, and they are calculated as

$$\mathbf{I} = \begin{bmatrix} \widetilde{\beta}\,(\mathbf{p}) \\ \widetilde{\gamma}\,(\mathbf{p}) \end{bmatrix}^\dagger \widetilde{\mathbf{B}}\,(\mathbf{p}) \quad (11)$$

where † represents the damped pseudoinverse, while $\widetilde{\beta}\,(\mathbf{p})$ and $\widetilde{\gamma}\,(\mathbf{p})$ contain the terms from (8) and (9) corresponding to the five components in $\widetilde{\mathbf{B}}$. The currents required to generate field and gradient at a given location ($\mathbf{p}$) within the workspace are obtained from (11). While the discussion here is specific to the BigMag system, the methodology can be generally applied to any system of electromagnetic coils.

III. SOFT ROBOTS

In this section, the designs of the magnetic soft robots are described in detail. This includes the design requirements, fabrication process and magnetization technique. Three different soft robots are designed for this work: two made of single strips of MPC, and another with six legs. All three soft robot designs and their dimensions are shown in Fig. 3. For the rest of this paper, these robots will be referenced as as *Worm-A*, *Worm-B* and *Hexapede*, respectively.

The soft robots are made from an MPC consisting of a silicone rubber matrix (Ecoflex-0010, Smooth-On Inc., USA) and a ferromagnetic powder of PrFeB with a mean particle size of 5μm (MQFP-16-7-11277, Magnequench GmbH, Germany). The mass ratio of the magnetic particles to the silicone rubber in the MPC is denoted by magnetic mass fraction (R). Once the components are mixed and degassed (to eliminate air bubbles), the MPC is allowed to cure in molds made from ABS or acrylic to form the shapes of the soft robots.

After the MPC sets, the soft robots are subjected to a large magnetization field so that the magnetic dipoles within the material align to specific directions. The interaction of these magnetic dipoles with the external magnetic field produces mechanical loads leading to motion of the soft robots. The magnetization is performed while holding the soft robots or their constituent components in jigs under a 1T field generated using a BE-25 electromagnet (Bruker Corp., USA). *Worm-A* (R = 1) and *Worm-B* (R = 2) are magnetized in molds of alternating semi-circular arcs. For *Hexapede* (R = 2), the legs are fabricated and magnetized first (for ease of magnetization), then the body is added and the entire robot is magnetized. The magnetization process is illustrated in Fig. 3.

In order to use the magnetic force to anchor the robots to

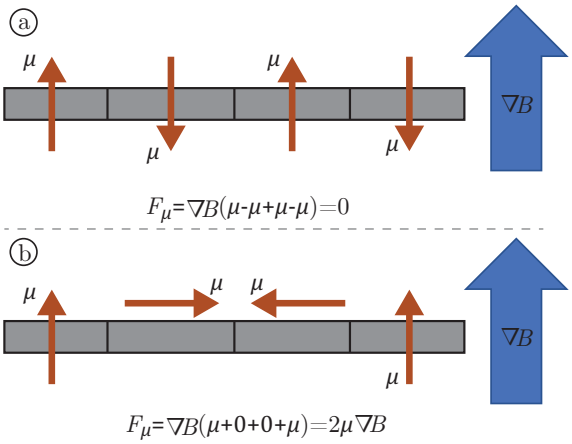

Fig. 4: ⓐ Schematic of a robot with four segments of alternating dipole moment orientations is shown. All the segments have dipoles of equal magnitude (μ). When subjected to a magnetic field gradient (∇B), the robot experiences a zero net magnetic force (F_μ) and therefore cannot be anchored using magnetic force. ⓑ The designs used in this paper are engineered to have a net magnetic dipole moment towards one direction, so that the robots can be anchored using magnetic field gradients.

a surface, it is preferable to design the robots to have a net magnetic dipole moment in one direction. This is illustrated in Fig. 4. If the soft robot has alternating dipoles (as seen in [8], [10], [11]), it results in low net magnetic force. Therefore, the robots used in this work are designed to have a net magnetic dipole moment towards a given direction. Additionally, it is beneficial to have the net dipole moment to be as high as possible, so that greater forces can be generated using smaller magnetic fields.

As part of the design process, it is necessary to determine if the electromagnetic system can generate forces sufficient to anchor the soft robots. As an example, *Hexapede* is considered to be anchored to the ceiling of the workspace, working against gravity. The body of *Hexapede* has a magnetization in the z-direction ($\mu = [0, 0, \mu_z]$). The magnetic powder has a residual flux density (B_r = 0.95T) after magnetization. The volume of the robot body is V = 18mm×2mm×6mm = 216mm^3. The volume of magnetic powder (V_μ) in the body is given by

$$V_\mu = V\frac{\rho_s R}{\rho_s R + \rho_\mu}, \tag{12}$$

where $\rho_s = 1040\text{kgm}^{-3}$ is the mass density of silicone rubber and $\rho_\mu = 7610\text{kgm}^{-3}$ is the theoretical mass density of magnetic powder. The magnitude of the dipole moment can be calculated as

$$\mu_z = \frac{1}{\mu_0} B_r V_\mu, \tag{13}$$

where $\mu_0 = 4\pi\times10^{-7}\text{Hm}^{-1}$ is the permeability of free space. The weight of the robot body is given by

$$W = gV\frac{(R+1)\rho_\mu\rho_s}{\rho_\mu + R\rho_s}, \tag{14}$$

where g is the acceleration due to gravity. The magnetic field gradient can anchor the robot body to the surface if the force generated by it is greater than the weight of the robot. Substituting the parameters for the robot body, and ignoring the off-diagonal terms of $\nabla\mathbf{B}$, we obtain $\partial B_z/\partial_z > 0.148\ \text{Tm}^{-1}$. BigMag can produce gradients greater than 0.5Tm^{-1}, which suggested that it was possible to demonstrate gradient-based anchoring of soft robots in this setup.

IV. EXPERIMENTS

In order to validate the concepts described in this paper, experiments are conducted in BigMag on each of the magnetic soft robots. For brevity, the notation ∇B_z will be used to describe the field gradient $\partial B_z/\partial_z$, and B_x and B_z for the field in the x and z directions, respectively. **The motion of the soft robots is shown in the supplementary video**.

In the first experiment, the ability to regulate the field and field gradient independently is demonstrated. For this, *Worm-A* is placed on the floor of the workspace (Fig. 5). It is first anchored to the ceiling using the field gradient, and then the magnetic field is varied in order to generate torques that cause the robot to flex between different shapes. At the start of the experiment, ∇B_z is set to a constant value of 0.3Tm^{-1}, with B_z at 20mT, causing the robot to anchor to the ceiling of the workspace in a 'W' shape. Changing the value of B_z while holding ∇B_z constant causes the robot to deform, alternating between the 'W' and 'U' shape, while being anchored to the ceiling. This demonstrates that the gradient and field can be controlled independently using the framework described in Sec. II-C.

The second experiment demonstrates locomotion of a soft robot while being anchored to the ceiling (Fig. 6). In order to generate locomotion, the *direction* of the magnetic field must be changed while maintaining sufficient field gradient to anchor the robot to the ceiling. In this case, *Hexapede* is placed on the floor of the workspace. At the start of the experiment, B_z = 10mT, B_x = 0mT and ∇B_z = 0.4Tm^{-1}, which forces the robot to be attached to the ceiling of the workspace. Then, the gradient is held steady while the magnetic field is rotated $\pm45°$ around the y-axis. The rotating field causes the legs to move forward in a cyclical manner that generates forward motion. However, it is observed that the gradient remains constant only within a small section of the workspace, outside of which the magnetic force is insufficient to hold the robot against gravity. Nonetheless, the experiment does demonstrate that ∇B_z can be kept sufficiently constant (at a high value) even when the direction of the magnetic field vector is changing.

The third experiment demonstrates the use of magnetic force to achieve locomotion on the ground. *Worm-B* is made of a thin strip of material that undergoes large deformation even when subjected to small magnetic torques. It cannot achieve locomotion using the magnetic field alone because the torque will cause the body to lift up off the surface. To overcome this, the magnetic field gradient is used to anchor the robot to the floor while the magnetic field is rotated to generate locomotion. For this, *Worm-B* is placed on the floor of the workspace, and ∇B_z is set to -0.1Tm^{-1} such that the robot is pressed into the floor (Fig. 7). Then, the magnetic field is rotated from the direction of $-x$ to $+x$ through 180° with a maximum magnitude of 20mT. This causes the robot body to deform, leading to peristaltic locomotion. This is a

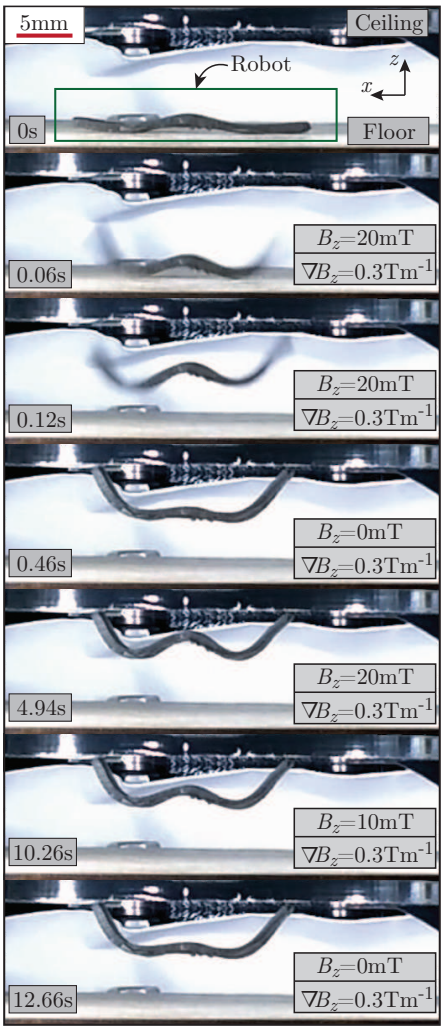

Fig. 5: Experiment demonstrating combined use of magnetic field and gradient along the z-axis. At the start of the experiment (0s), *Worm-A* is on the floor of the workspace. Upon application of magnetic force (0.06s), it is anchored to the ceiling of the workspace (0.46s). Thereafter, varying the magnetic field (B_z) while maintaining the field gradient (∇B_z) causes the robot to flex between 'U'-shape and 'W'-shape. **See supplementary video.**

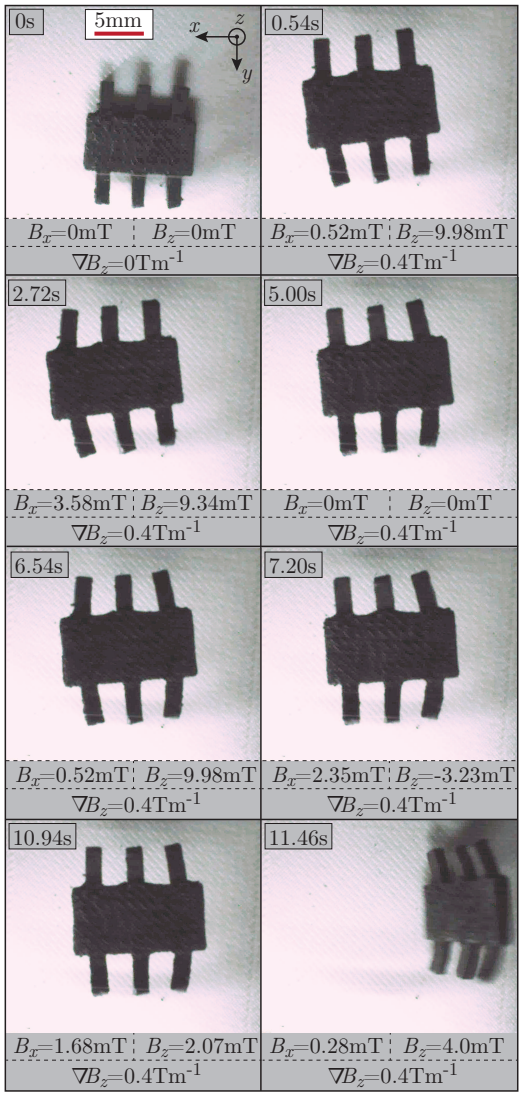

Fig. 6: Experiment showing motion of *Hexapede* robot while anchored to the ceiling of the workspace. At the start of the experiment (0s), the robot is on the floor of the workspace. It is then anchored to the ceiling (0.54s) using the magnetic field gradient (∇B_z). By rotating the magnetic field (B_x and B_z), the legs move back and forth to generate locomotion. In the last frame, the robot is seen detaching from the ceiling since the anchoring magnetic force is insufficient in that region of the workspace (11.46s). **See supplementary video.**

particular scenario in which the magnetic force constrains the robot to stay attached to the floor, while the magnetic torque causes some parts of the robot body to lift off the floor.

A. Discussion

The experiments described above validate the methodology presented here for the combined field and gradient generation as a proof-of-concept. However, the motion of the soft robots shown here is restricted to a small area of the workspace. There are specific technical bottlenecks that prevent demonstration of large-scale motion. For the discussion here, plots of the magnetic field and field gradient at various stages during the experiments are shown in Fig. 8.

First, the field gradients are sufficiently high only in the proximity of the coils. This is expected as the magnetic field decays with the third power of the distance from the source (a coil, in this instance), whereas the field gradient decays by the fourth power of the distance. Second, the other components of the field gradient matrix gain prominence outside a small working area close to the axis of the top coil, as noticed in Fig. 8ⓔ,ⓕ. Therefore, once the robot locomotes for a few cycles, it is also affected by forces in the x or y directions that destabilize the anchored motion of the robot. One way to combat this issue may be to have a moving coil that can adjust its position to follow the robot throughout the motion. Additionally, the power required to generate large fields and gradients is quite high, particularly for cases like *Worm-B*, where the field and gradient act in opposite directions (Fig. 8ⓒ,ⓕ). In BigMag, the coils are limited to 10A of current, which limits the forces and torques that can be generated.

One solution to many of these issues is to design electromagnetic systems with more coils. This provides more actuation degrees of freedom, allowing the possibility to regulate more elements of the gradient matrix. Also, this can

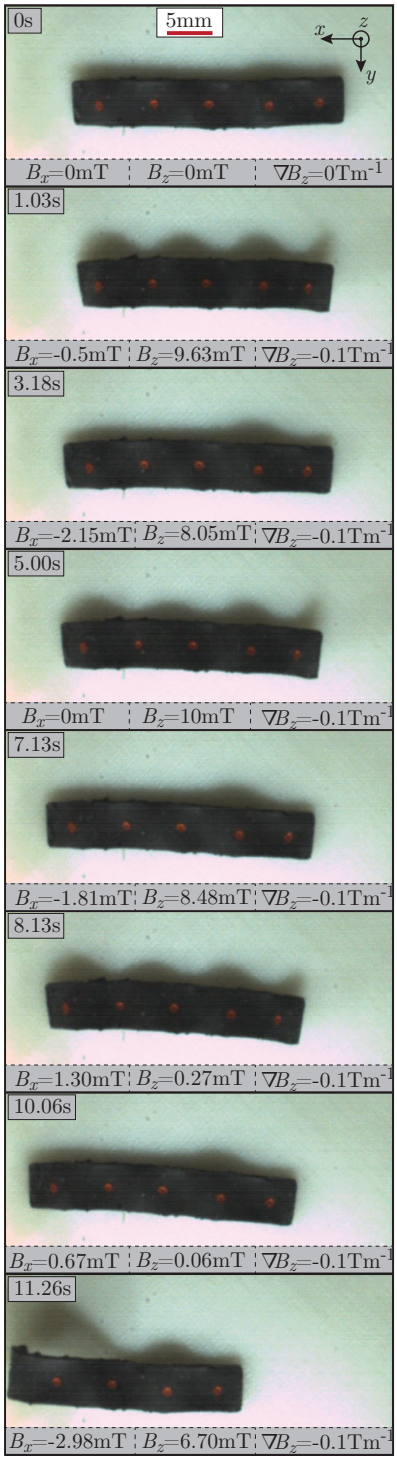

Fig. 7: Experiment demonstrating motion of *Worm-B* robot on the floor of the workspace under actuation using combined magnetic force and torque. At the start (0s), the robot is resting on the floor of the workspace. In the next frame (1.03s), the magnetic force is pushing the robot into the floor, while the magnetic torque causes deformation of the body. Thereafter, rotating the magnetic torque while maintaining the magnetic force generates peristaltic locomotion. In the final frame (11.26s), the robot is pulled to the edge of the workspace due to magnetic force in the x-direction. **See supplementary video.**

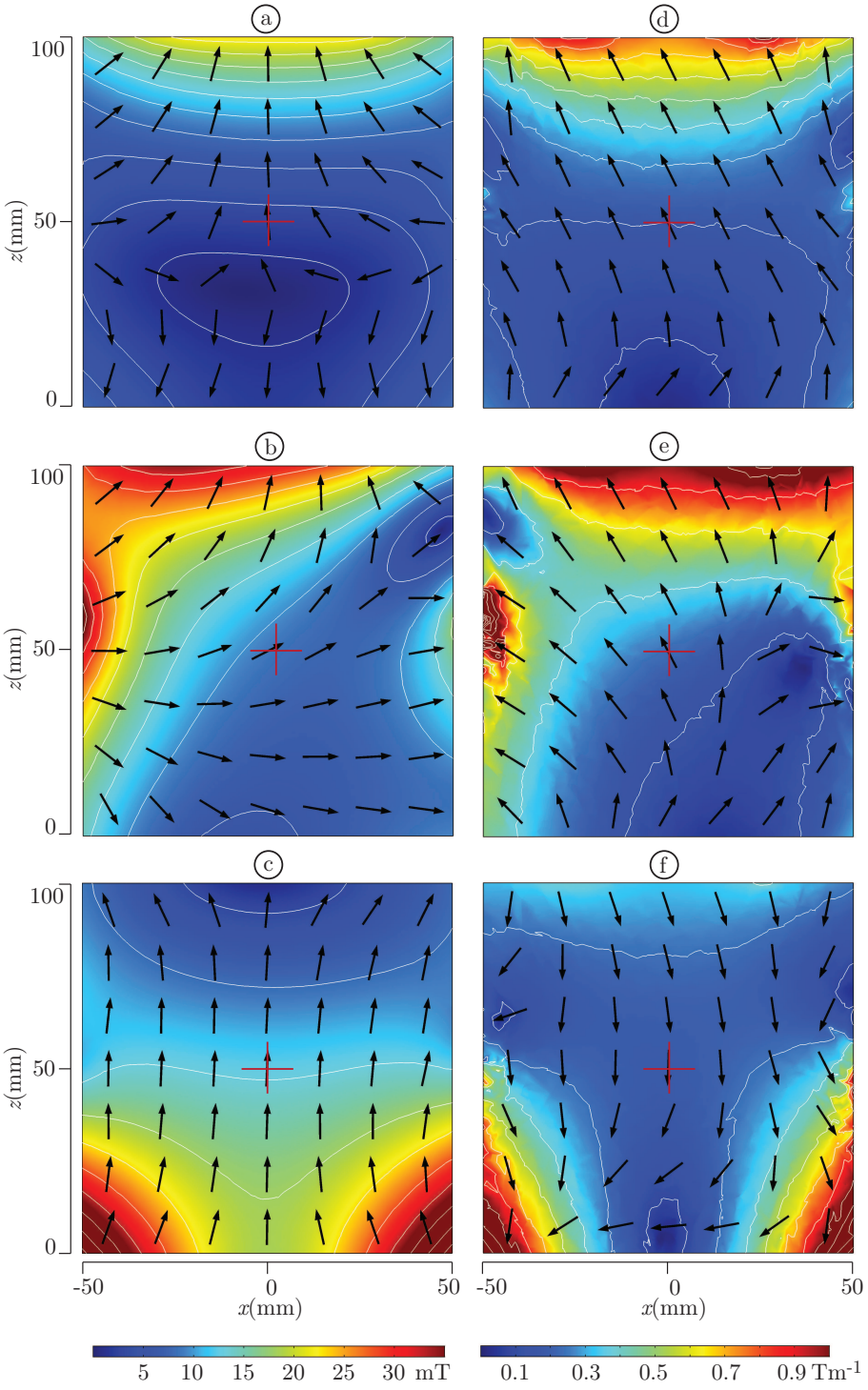

Fig. 8: Plots of magnetic field (ⓐ-ⓒ) and field gradient (ⓓ-ⓕ) in the x-z plane of the workspace during the experiments described in Sec. IV. Colors and contours denote the magnitude while arrows represent the direction of the vectors. At the start of each experiment, the robot is at the center of the workspace (x=0mm, z=50mm) denoted by the cross-hairs. ⓐ,ⓓ: In the first experiment, the magnetic field and field gradient act in the same direction ($+z$). Therefore, the direction of the gradient is fairly uniform within the workspace, leading to stable anchoring. ⓑ,ⓔ: During the second experiment, the magnetic field points towards the $+x$ direction, leading to nonuniform gradients that destabilize the robot during locomotion. ⓒ,ⓕ: In the final experiment, the field and gradient act in opposite directions ($+z$ and $-z$, respectively), leading to higher power consumption in the coils. Plots were generated in COMSOL Multiphysics 5.4, Comsol Inc., USA.

help distribute the electrical load more evenly, empowering the system to produce greater actuation loads. Another possibility is to use coils with cooling systems. However, fitting many high-power coils and cooling systems around a workspace presents a logistical challenge.

Another option is to miniaturize the robots themselves. This has inherent benefits if the intended application is minimally invasive surgery, since smaller robots can potentially navigate restricted areas of the human body. While the robots shown here are fabricated using bench-top techniques, additive manufacturing presents opportunities for creating milli- and micro-scale soft robots. While some works in literature have proposed methods for additive manufacturing of small-scale magnetic soft robots, it is necessary to improve the magnetic density within the structures in order to achieve anchoring using magnetic field gradients.

The robots in this work are treated as concentrated magnetic masses, whereas in reality the magnetic dipoles are spread across the continuum of each robot body. Also, no models are developed for theoretical estimation of the motion of these robots. Both of these aspects must be addressed to achieve improved control over these types of soft robots.

V. CONCLUSIONS

In this paper, actuation of soft robots using magnetic torque in conjunction with magnetic force is demonstrated as a proof-of-concept. Three different soft robots are presented, and are subjected to separate experiments to demonstrate different scenarios of the combined force and torque actuation. The main contribution of this work is the demonstration of various types of robot motion while ensuring the robots remain anchored to the working surface through magnetic forces. *Hexapede* and *Worm-A* are anchored to the ceiling, counteracting gravity, while *Worm-B* is anchored to the floor of the workspace in order to produce locomotion.

The methodology described here is used for actuation using a six-coil electromagnetic system, but is also applicable to other coil-based systems. Due to physical restrictions of the setup, only small motions of the robots are demonstrated here. In order to achieve better control of the actuation, it is necessary to develop actuation units with higher power capacities and more degrees of freedom.

In the future, miniaturization of the robots through additive manufacturing methods will be investigated. By incorporating bio-compatible materials and other functional elements (e.g. drug release in response to chemical or thermal stimulus), it is possible to make the robots suitable for minimally invasive surgical procedures. Developing sensing technologies for localization of the robots within an enclosed environment would truly move them towards fully untethered operation.

REFERENCES

[1] D. Rus and M. T. Tolley, "Design, fabrication and control of soft robots," *Nature*, vol. 521, no. 7553, pp. 467–475, May 2015.

[2] S. Kim, C. Laschi, and B. Trimmer, "Soft robotics: a bioinspired evolution in robotics," *Trends in biotechnology*, vol. 31, no. 5, pp. 287–294, 2013.

[3] S. Seok, C. D. Onal, K. Cho, R. J. Wood, D. Rus, and S. Kim, "Meshworm: A Peristaltic Soft Robot With Antagonistic Nickel Titanium Coil Actuators," *IEEE/ASME Transactions on Mechatronics*, vol. 18, no. 5, pp. 1485–1497, Oct. 2013.

[4] R. F. Shepherd, F. Ilievski, W. Choi, S. A. Morin, A. A. Stokes, A. D. Mazzeo, X. Chen, M. Wang, and G. M. Whitesides, "Multigait soft robot," *Proceedings of the National Academy of Sciences*, vol. 108, no. 51, pp. 20 400–20 403, Dec. 2011.

[5] H.-W. Huang, M. S. Sakar, A. J. Petruska, S. Pané, and B. J. Nelson, "Soft micromachines with programmable motility and morphology," *Nature Communications*, vol. 7, p. 12263, Jul. 2016.

[6] V. Q. Nguyen, A. S. Ahmed, and R. V. Ramanujan, "Morphing Soft Magnetic Composites," *Advanced Materials*, vol. 24, no. 30, pp. 4041–4054, Aug. 2012.

[7] G. Z. Lum, Z. Ye, X. Dong, H. Marvi, O. Erin, W. Hu, and M. Sitti, "Shape-programmable magnetic soft matter," *Proceedings of the National Academy of Sciences*, vol. 113, no. 41, pp. E6007–E6015, Oct. 2016.

[8] E. Diller, J. Zhuang, G. Z. Lum, M. R. Edwards, and M. Sitti, "Continuously distributed magnetization profile for millimeter-scale elastomeric undulatory swimming," *Applied Physics Letters*, vol. 104, no. 17, p. 174101, 2014.

[9] Y. Kim, G. A. Parada, S. Liu, and X. Zhao, "Ferromagnetic soft continuum robots," *Science Robotics*, vol. 4, no. 33, p. eaax7329, Aug. 2019.

[10] W. Hu, G. Z. Lum, M. Mastrangeli, and M. Sitti, "Small-scale soft-bodied robot with multimodal locomotion," *Nature*, vol. 554, no. 7690, pp. 81–85, Feb. 2018.

[11] V. K. Venkiteswaran, L. F. P. Samaniego, J. Sikorski, and S. Misra, "Bio-Inspired Terrestrial Motion of Magnetic Soft Millirobots," *IEEE Robotics and Automation Letters*, vol. 4, no. 2, pp. 1753–1759, Apr. 2019.

[12] M. P. Kummer, J. J. Abbott, B. E. Kratochvil, R. Borer, A. Sengul, and B. J. Nelson, "OctoMag: An Electromagnetic System for 5-DOF Wireless Micromanipulation," *IEEE Transactions on Robotics*, vol. 26, no. 6, pp. 1006–1017, Dec. 2010.

[13] A. J. Petruska and J. J. Abbott, "Omnimagnet: An Omnidirectional Electromagnet for Controlled Dipole-Field Generation," *IEEE Transactions on Magnetics*, vol. 50, no. 7, pp. 1–10, Jul. 2014.

[14] J. Sikorski, I. Dawson, A. Denasi, E. E. G. Hekman, and S. Misra, "Introducing BigMag - A novel system for 3d magnetic actuation of flexible surgical manipulators," in *2017 IEEE International Conference on Robotics and Automation (ICRA)*, May 2017, pp. 3594–3599.

[15] J. Sikorski, C. M. Heunis, F. Franco, and S. Misra, "The ARMM System: An Optimized Mobile Electromagnetic Coil for Non-Linear Actuation of Flexible Surgical Instruments," *IEEE Transactions on Magnetics*, vol. 55, no. 9, pp. 1–9, Sep. 2019.

[16] G. Ciuti, P. Valdastri, A. Menciassi, and P. Dario, "Robotic magnetic steering and locomotion of capsule endoscope for diagnostic and surgical endoluminal procedures," *Robotica*, vol. 28, no. 2, pp. 199–207, Mar. 2010.

[17] H. Lu, M. Zhang, Y. Yang, Q. Huang, T. Fukuda, Z. Wang, and Y. Shen, "A bioinspired multilegged soft millirobot that functions in both dry and wet conditions," *Nature Communications*, vol. 9, no. 1, p. 3944, Sep. 2018.

[18] M. Simi, M. Silvestri, C. Cavallotti, M. Vatteroni, P. Valdastri, A. Menciassi, and P. Dario, "Magnetically Activated Stereoscopic Vision System for Laparoendoscopic Single-Site Surgery," *IEEE/ASME Transactions on Mechatronics*, vol. 18, no. 3, pp. 1140–1151, Jun. 2013.

[19] G. Pittiglio, L. Barducci, J. W. Martin, J. C. Norton, C. A. Avizzano, K. L. Obstein, and P. Valdastri, "Magnetic Levitation for Soft-Tethered Capsule Colonoscopy Actuated With a Single Permanent Magnet: A Dynamic Control Approach," *IEEE Robotics and Automation Letters*, vol. 4, no. 2, pp. 1224–1231, Apr. 2019.

[20] E. Diller, J. Giltinan, and M. Sitti, "Independent control of multiple magnetic microrobots in three dimensions," *The International Journal of Robotics Research*, vol. 32, no. 5, pp. 614–631, Apr. 2013.

[21] E. Diller, J. Giltinan, G. Z. Lum, Z. Ye, and M. Sitti, "Six-degree-of-freedom magnetic actuation for wireless microrobotics," *The International Journal of Robotics Research*, vol. 35, no. 1-3, pp. 114–128, Jan. 2016.

[22] A. J. Petruska and B. J. Nelson, "Minimum Bounds on the Number of Electromagnets Required for Remote Magnetic Manipulation," *IEEE Transactions on Robotics*, vol. 31, no. 3, pp. 714–722, Jun. 2015.